Available online at www.sciencedirect.com
SCIENCE DIRECT®
Polymer 45 (2004) 3755–3763
polymer
www.elsevier.com/locate/polymer

Melting and reorganization of poly(ethylene terephthalate) on fast heating (1000 K/s)

Alexander A. Minakov[1], Dmitry A. Mordvintsev, Christoph Schick*

Department of Physics, University of Rostock, Universitätsplatz 3, 18051 Rostock, Germany

Received 30 December 2003; received in revised form 18 March 2004; accepted 23 March 2004

Abstract

For poly(ethylene terephthalate) (PET) and other polymers the origin of the multiple melting peaks observed in differential scanning calorimetry (DSC) curves is still controversially discussed. This is due to the difficulty to investigate the melting of the originally formed crystals exclusively. Recrystallization is a fast process and most experimental techniques applied so far do not allow fast heating in order to prevent recrystallization totally. Developments in thin-film (chip) calorimetry allow scanning rates as high as several thousand Kelvin per second. We utilized a chip calorimeter based on a commercially available vacuum gauge, which is operated under non-adiabatic conditions. The calorimeter was used to study the melting of isothermally crystallized PET. Our results on melting at rates as high as 2700 K/s give clear evidence for the validity of a melting–recrystallization–remelting process for PET at low scanning rates (DSC). At isothermal conditions PET forms crystals, which all melt within a few dozens of K slightly above the isothermal crystallization temperature. There is no evidence for the formation of different populations of crystals with significantly different stability (melting temperatures) under isothermal conditions. Superheating of the crystals is of the order of 10 K at 2700 K/s.
© 2004 Published by Elsevier Ltd.

Keywords: Polymer crystallization; Multiple melting; Fast calorimetry

1. Introduction

A lamellar stack model describes the morphology of most semicrystalline polymers reasonable well. Although this morphology feature was discovered already 65 years ago [1] the question how polymer crystals are formed is still under debate (see e.g. Refs. [2–6] and references therein). It is the chain structure of the polymer molecules, which forces polymers to form morphologies, build up from folded chain lamellae and spherulites. Because the equilibrium structure—the extended chain crystal—is commonly not realized, these structures are not in thermodynamic equilibrium. The deviation from equilibrium causes significant reorganization and recrystallization already at crystallization or at annealing and heating [7]. All this makes a description of polymer crystallization and melting a very complex task. Crystallization at large super cooling yields structures, which are especially far from thermodynamic equilibrium. Melting–recrystallization–remelting sequences are often considered to describe the complex melting behaviour of polymers crystallized under such conditions. Calorimetry and especially differential scanning calorimetry (DSC) is commonly applied to study polymer melting. Other techniques like temperature dependent X-ray diffraction [7] or in situ atomic force microscopy (AFM) [8–11] support the idea of melting–recrystallization. But other models like the creation of secondary lamella or the relaxation of the rigid amorphous fraction are considered too to describe the multiple melting peaks occurring in DSC curves [12–15].

For several polymers like poly(ethylene terephthalate) (PET) the issue is still not finally resolved even though it was studied already in 1970 [16]. To investigate the melting of the originally formed crystals exclusively is difficult because recrystallization is a fast process and most experimental techniques applied so far do not allow fast heating in order to prevent recrystallization totally. Sauer et al. showed that PET crystallized at low temperatures

* Corresponding author. Tel.: +49-381-498-6880, fax: +49-381-498-6882.
E-mail address: christoph.schick@physik.uni-rostock.de (C. Schick).
[1] On leave from the Natural Science Research Centre of A. M. Prokhorov General Physics Institute of Russian Academy of Science, Vavilov st. 38, 119991 Moscow, Russia.

0032-3861/$ - see front matter © 2004 Published by Elsevier Ltd.
doi:10.1016/j.polymer.2004.03.072

becomes liquid-like according to viscosity at relatively low melting temperatures [17]. Robertson et al. [18] showed by special temperature sequences in DSC experiments for poly(butylene terephthalate) (PBT) that recrystallization is about two orders of magnitude faster than isothermal crystallization at the same temperature. To study exclusively the melting of the originally present crystals in a polymer sample, consequently, requires very high heating rates. Pijpers et al. extended the heating and cooling rate range of DSC to rates as high as 500 K/min (Hyper DSC™) [19]. But for commercial PET these rates are still not high enough to prevent recrystallization as shown below.

Developments in thin-film (chip) calorimetry [20,21] allow much higher rates also for low thermal conducting polymer samples as recently shown by Allen et al. [22–24]. We have developed a chip calorimeter [25,26] based on a commercially available vacuum gauge TCG 3880 from Xensor Integration, Nl, [27]. A thin-film thermopile is used as thermometer and placed on a thin Si_3N_x membrane with a film heater. The measurements are performed in an ambient gas atmosphere rather than under adiabatic conditions. Therefore, measurements on controlled cooling are possible too [25,26]. The calorimeter allows rates up to several thousand Kelvin per second and was applied here to study the melting of isothermally crystallized PET.

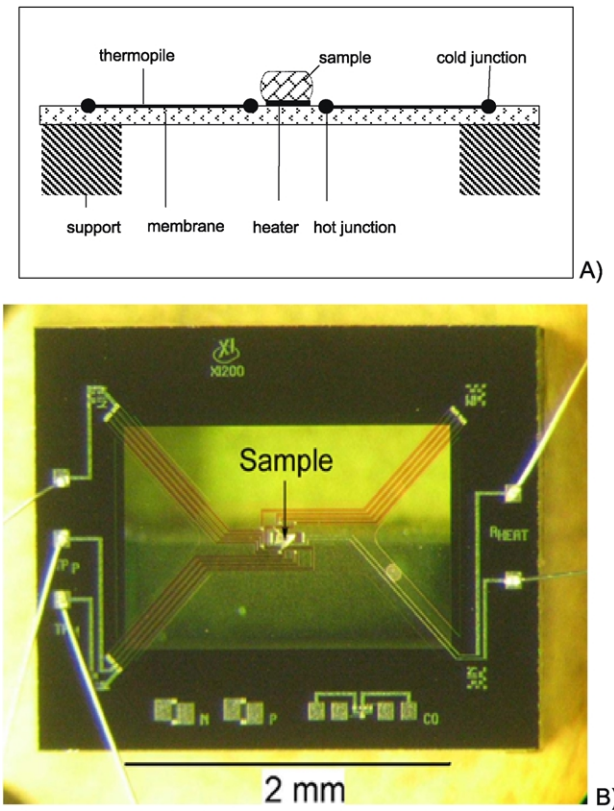

Fig. 1. Thin-film chip calorimeter based on the thermal conductivity gauge TCG-3880. Scheme (A) and micro photograph of the frame and the membrane loaded with a sample (B).

2. Experimental

The PET sample was from KoSa GmbH and Co. KG, Germany, and had a molecular weight of 44,000 Da. From the amorphous granule a tiny peace of the order of a few hundred nanograms was cut. The sample was moved on top of the heater of the calorimetric sensor, see Fig. 1. To avoid damaging of the sensor membrane (ca. 1 μm thick) the sample was moved by a soft cooper wire (diameter 50 μm). A stereo microscope was used to control the movement. When the sample was on the right place an electrical current through the heater was switched on to melt the sample for the first time. This way the sample was fixed at a position just on top of the heater. Because of strong adhesive forces the sample-membrane thermal contact after a few heating–cooling cycles was good and very stable, which is important for calorimetric measurements [28,29].

The thermal conductivity gauge TCG-3880 [27] shown in Fig. 1 consists of 0.5 μm Si_3N_x membrane with a thin-film thermopile and a resistive film-heater placed at the center of the membrane. All electrical connections are covered by an additional 0.7 μm SiO_2 layer for electrical isolation and protection. The six thermopile hot junctions—the white spots around the central region in the photograph—are placed around the central heated area, ca. 50×100 μm^2. The cold junctions are placed at the silicon frame fixing the membrane, ca. 1 mm from the center. Thus the cold-junction temperature equals the temperature of the holder, which is close to the temperature of the thermostat. An additional copper-constantan thermocouple was utilized for the measurement of the holder temperature, which was used as the reference temperature T_0.

To allow fast cooling the cell was operated in an ambient gas. The heat flow from the heated region to the environment can be described by Newton's law: $\Phi = \xi \Delta T$, where Φ is the heat flow from the heated region, ξ is the heat exchange parameter measured in W/K and $\Delta T = (T - T_0)$, where T is the temperature of the heated region of the membrane, T_0 is the temperature of the environment, which is close to the temperature of the holder. The heat exchange parameter ξ equals ca. 2×10^{-5} W/K in air atmosphere at pressures in the range 10^2–10^5 Pa and room temperature [25]. The parameter ξ is six times larger, when the calorimeter is operated in helium gas. Because the membrane is very thin the heat transfer through the ambient gas is dominant. The heat transfer through the membrane in radial direction is at least 10 times smaller than that through the gas in the perpendicular direction [25]. The measurements can be performed at atmospheric pressure, as well as at pressures in the range 10–10^5 Pa, where the gas thermal conductivity is still relatively large. In fact, the measurements were performed in air at 2×10^3 Pa.

The expected maximal cooling rate $(dT/dt)_{max}$ of a 500 ng sample, with heat capacity C ca. 500 nJ/K, can be estimated as follows: $(dT/dt)_{max} = \Delta T \xi/(C + C_0)$. The

addenda heat capacity C_0 equals ca. 150 nJ/K at room temperature [25]. Thus, $(dT/dt)_{max}$ is of the order of 2×10^4 K/s at $\Delta T = 500$ K, which was confirmed experimentally [25,26]. Linear cooling is only possible, when the scanning rate is several times smaller than $(dT/dt)_{max}$. On the other hand, sample thickness d must be small enough to avoid a large temperature gradient in the sample. The temperature difference δT across a plate-like sample can be estimated as follows: $\delta T = (dT/dt)(d^2\rho c/\lambda)$, where ρ, c and λ are the density, the specific heat capacity and the thermal conductivity of the sample, respectively. Thus, δT equals 1–3 K at $d = 10$ μm and $dT/dt = 3 \times 10^3$ K/s for PET with $c = 1 - 2$ J/gK [30], $\rho = 1.3$ g/cm^3 and λ ca. 0.3 W/K m [31]. As a temperature gradient exists in the radial direction along the membrane, the sample should be placed just on the heater. Otherwise, there will be a temperature gradient on the periphery of the sample outside the heated area.

The thermal contact between the heater and the thin PET sample is sufficiently good due to strong adhesive forces. Nevertheless, the measured temperature does not represent the temperature of the heater/sample interface, because the thermopile measures the temperature at the membrane around the heater. Thus the measured temperature was calibrated as described in Ref. [25]. The heat capacities and thermal resistances of the film-heater and of the thermopile are negligibly small. The addenda heat capacity is, therefore, the effective heat capacity of the heated part of the membrane. Thus, the sample-membrane system can be described by the following parameters: the effective heat capacity of the central part of the membrane C_0, the heat capacity of the sample C and the heat-exchange coefficient ξ. The resistive film-heater, ca. 600 Ohm, provides the heat flow $\Phi_0(t)$, which is supplied to the membrane/sample interface and propagates through the sample, the membrane and the ambient gas. The heat balance equation is as follows:

$$(C + C_0)dT/dt = \Phi_0(t) - \xi \times (T(t) - T_0), \quad (1)$$

this equation is correct, provided the thermal thickness of the sample is small enough, and the heat transfer from the sample to the thermostat can be described by Newton's law. The temperature measured by the thermopile is ca. 10 ms delayed with respect to the heater current [25]. The duration of a cooling or heating scan must be large enough with respect to the delay time $\tau_0 \approx 10$ ms, otherwise we have to consider thermal waves rather than a monotonous heating or cooling process. Thus, the scanning rate must be much smaller than $\Delta T/\tau_0 \approx 5 \times 10^4$ K/s at $\Delta T = 500$ K. This limitation is of the same order of magnitude as the restriction, which follows from the limited heat exchange through the gas. In the present work the scanning rate was less than 3×10^3 K/s, i.e. the rate was ca. 10 times smaller compared to both limits. The heat flow $\Phi_0(t)$ is determined by the electric current in the heater, $I_H(t)$, and its resistance $R_H(T)$. The resistance $R_H(T)$ was calibrated in advance. The electric current in the heater was monitored during its scanning simultaneously with the temperature difference $T(t) - T_0$, measured by the thermopile. The temperature dependence of the thermopile sensitivity, S ca. 1 mV/K, and the thermopile thermal lag were calibrated as described in Ref. [25].

Thus, there are three unknown parameters in Eq. (1)—ξ, C_0 and C. The parameter $C_0(T)$ was determined in advance for the empty cell. It increases monotonously from ca. 100 to 200 nJ/K in the temperature range 100 to 600 K. The parameters ξ and C can be determined from heating–cooling scans as described in Ref. [25]. As the gas thermal conductivity depends on temperature, the heat exchange coefficient ξ is also a function of temperature. The dependence $\xi(T)$, which can be approximated by a smooth monotonous polynomial function [25], was determined as follows. First the heating–cooling cycle for an amorphous sample was investigated. Outside the glass transition range the heat capacity on cooling equals heat capacity on heating. This was used to determine $\xi(T)$. Therefore, the dependences $C(T)$ and $\xi(T)$ were determined simultaneously from cooling and heating curves for an amorphous sample. Next, the heat capacity of the crystallized sample was obtained on heating assuming the same dependence $\xi(T)$ as in the previous experiment, provided the gas pressure was kept constant. In order to determine the specific heat capacity, $c = C/m$, the sample mass m has to be known. The mass was not measured independently, because it was too small (100 ng). It was obtained from the measured heat capacity and the known specific heat capacity in the molten state at temperatures above 280 °C [30].

The current in the heater and the signal from the thermopile were monitored in real time during fast scanning of the membrane temperature as described in Ref. [25]. To simplify the analysis of the time dependences $T(t)$ and dT/dt we tried to scan temperature almost linearly with time. A function generator, Stanford Research Systems DS 340, was utilized to realize approximately constant scanning rate. The generator output voltage supplied to the heater was proportional to the square root of time. The data acquisition and control electronics are described in Ref. [26]. The temperature of the thermostat was stabilized at $T_0 = 30$ °C. The scanning range was ca. 350 K.

DSC and Hyper DSC™ measurements were performed utilizing a PerkinElmer Pyris Diamond DSC equipped with an Intracooler II and nitrogen as purge gas. The instrument was calibrated by indium and zinc for temperature at the scanning rate of interest and by sapphire for heat flow. The sample was wrapped in aluminum foil of a few mg only to minimize thermal lag [19].

First the crystallization time t_C for each crystallization temperature T_C was chosen such that primary crystallization was completed. For DSC measurements the samples were crystallized from the melt (melt crystallization). For the fast scanning experiments (chip calorimeter) the samples were quenched below glass transition before crystallization (cold crystallization) in order to allow a simpler scanning

program. No difference between cold and melt crystallization was observed because of the very high cooling and heating rates applied.

3. Results

The multiple melting peaks in isothermally crystallized PET are well known since long time [16]. Fig. 2 shows typical DSC curves for PET crystallized at different crystallization temperatures T_C. At large super cooling (low T_C) a low and a high melting endotherm is observed. At lower super cooling (high T_C) even multiple melting peaks are seen.

As commonly discussed the second melting peak for PET is the result of continues melting–recrystallization–remelting. Therefore, the second melting peak should disappear when recrystallization could be prevented by fast heating, provided at the initial isothermal crystallization, a monomodal population of lamellae was formed only. In order to check this, we performed experiments at different heating rates.

3.1. HyperDSC™ measurements

The results from DSC measurements at heating rates up to 500 K/min for samples melt crystallized at 210 and 130 °C are shown in Fig. 3.

For the PET sample melt crystallized at 210 °C, Fig. 3(A), a very complex melting behaviour is observed. At the two lowest heating rates two melting peaks at 260 °C and 250 °C, and a broad shoulder around 240 °C appears. The high temperature melting peak decreases at increasing heating rate and disappears as a separate peak at heating rate 20 K/min. At higher rates the shoulder at 240 °C develops and finally only one single peak is observed. The low

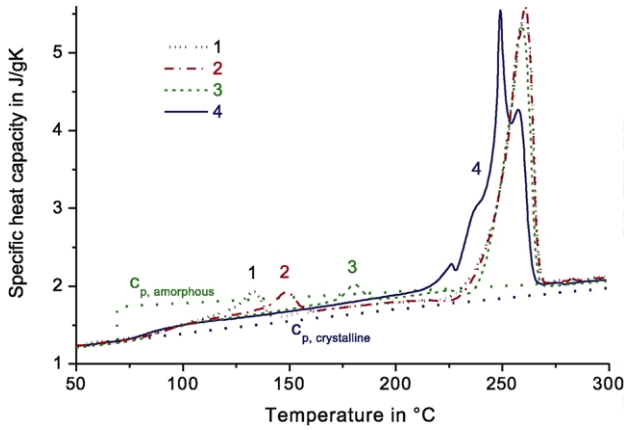

Fig. 2. Temperature dependences of the specific heat capacity of a 12 mg PET sample in the melting region at heating rate 20 K/min (0.3 K/s). The sample was crystallized at $1 - T_C = 210$ °C, $t_C = 1$ h; 2–170 °C, 5 min; 3–130 °C, 1 h; 4–110 °C, 8 h, and quenched below glass transition. The curves for completely amorphous and crystalline PET according to Ref. [30] are shown by dotted lines.

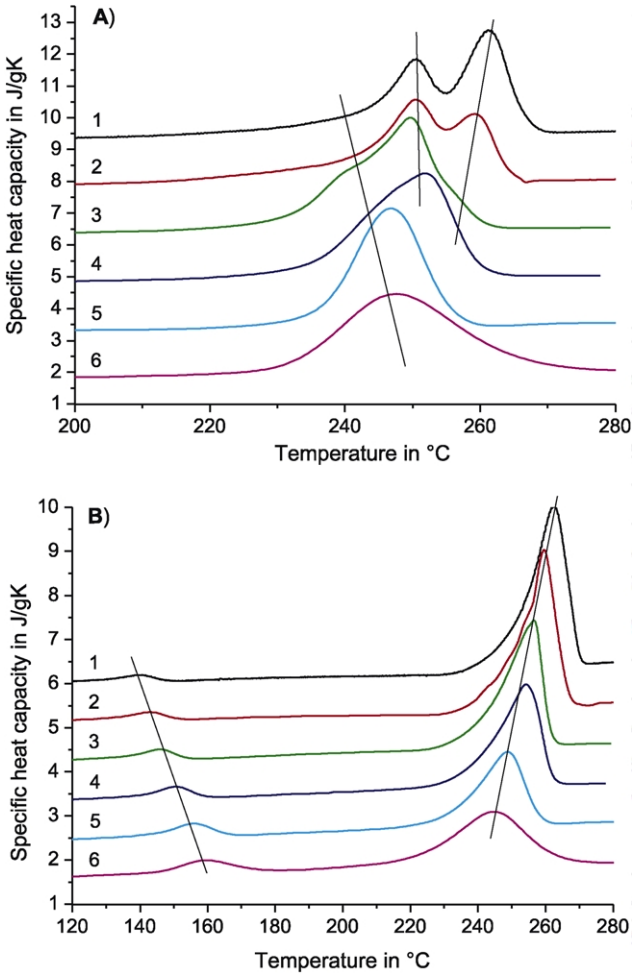

Fig. 3. Temperature dependences of the specific heat capacity of 0.5–16 mg PET samples at the following heating rates: 1–2 K/min (0.033 K/s) 16 mg, 2–5 K/min (0.083 K/s) 16 mg, 3–20 K/min (0.33 K/s) 6 mg, 4–50 K/min (0.83 K/s) 6 mg, 5–200 K/min (3.3 K/s) 0.5 mg, 6–500 K/min (8.3 K/s) 0.5 mg. The samples were crystallized at 210 °C (A) and 130 °C (B) for 1 h. The curves are vertically shifted and the straight lines are guides to the eyes only.

temperature peak at 240 °C is hidden at low heating rates because of continuous melting and recrystallization. Why we see two peaks at higher temperatures at low heating rates is not well understood. But all these peaks disappear at high heating rates. Obviously, there is no indication for any multimodal distribution in melting temperatures etc. For the crystallization temperature of 210 °C the rate of 200 K/min (ca. 3 K/s) is fast enough to reach some limiting curve shape. The crystals formed at 210 °C do not recrystallize very fast. Therefore, 200 K/min is fast enough to prevent recrystallization. The crystals formed at 130 °C, Fig. 3(B), are less stable. Therefore, even at 500 K/min two well separated peaks are seen. But the increasing low temperature peak and the shift of the second melting peak towards lower temperatures with increasing heating rate strongly support the melting–recrystallization–remelting model also for this sample. Obviously, 500 K/min is not fast enough to prevent recrystallization.

3.2. Chip calorimeter measurements

In order to increase heating rate even more, we used the chip calorimeter described in the experimental part. The PET sample of 360 ng was molten at 340 °C for a very short time to minimize degradation of the sample. During heating and cooling at 2700 K/s the sample was subjected to temperatures above 300 °C for 30 ms only. After isothermal cold crystallization the sample was quenched again below glass transition at 30 °C. The quenching rate was 10^4 K/s. Then the measurements were performed at different scanning rates. The melting curves and the subsequent cooling curves at the same rates are shown in Fig. 4. Dramatic changes in the shape of the melting peaks appear depending on heating rate. On cooling no crystallization occurs and the glass transition of the amorphous PET is seen.

To verify the estimates for the temperature gradients across the sample and the calibration applied, see Section 2, we first checked the influence of thermal lags on the curves at different high rates. The dynamic calorimetric glass transition temperature is known to depend on frequency according a Vogel–Fulcher–Tamman–Hesse equation [32]. The same is true for the cooling rate dependence because cooling rate can be transformed to frequency according $f = q/2\pi a\delta T$ [33] where q is cooling rate in K/s, a is a constant of ca. 6 [34] and δT the mean temperature fluctuation, which can be extracted from the width of the glass transition interval. For the amorphous PET δT is about 2 K. Then a cooling rate of 150 K/s corresponds to a frequency of about 2 Hz and at 2700 K/s to about 36 Hz. For the semicrystalline sample δT is about 10 K resulting in frequencies between 0.4 and 7 Hz. In Fig. 5, the glass transition temperatures are shown together with the VFT fits from dielectric experiments [35].

From Fig. 5, we see that the glass transition temperatures are in the expected temperature range except the single value at heating at 1100 K/s for the semicrystalline sample. For the cooling rate range covered here, we would expect a shift in glass transition temperature of about 6 K for the amorphous sample [35,36]. Such a shift is indicated by the horizontal bar in the inset in Fig. 4. The shift is not clearly seen in the inset in Fig. 4. Fig. 5 shows that uncertainty in glass transition temperature is about ± 10 K, which is due to the uncertainty of the determination of T_g (ca. ± 5 K) and the uncertainty of the temperature measurement (ca. ± 5 K) as estimated above.

Although the temperature measurement is not very precise it is good enough to study melting and reorganization of PET as shown in Fig. 4. For the two lowest rates two separate melting peaks are observed. The high temperature peak decreases with increasing heating rate and shifts to lower temperature as for the DSC measurements, see Fig. 3(A). At 1100 K/s only a shoulder remains at the high temperature flank. Even at rates of 2700 K/s the melting peak shows a slight shoulder. It may be explained by reorganization during the scan or a broad distribution in crystal stability (melting points), which may exist for the crystals initially formed at 133 °C. To check this we tried to measure at even higher rates. In order to do so we had to reduce sample mass further. Unfortunately, sample thickness became so thin that surface effects could not longer be neglected. The effect of sample thickness, which was estimated from sample mass and sample area, is shown in Fig. 6.

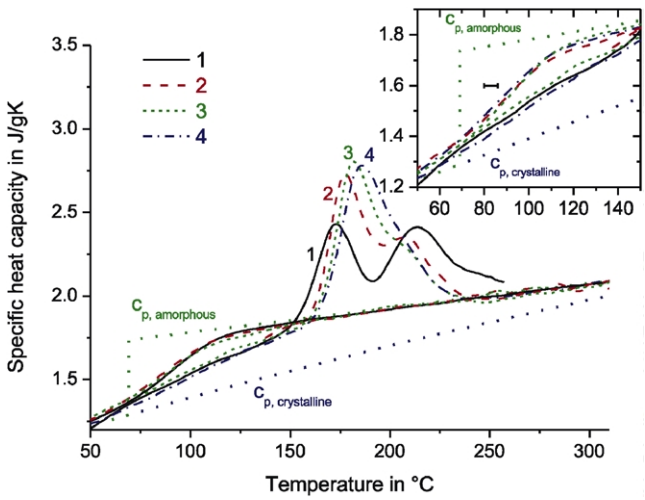

Fig. 4. Temperature dependences of the specific heat capacity of 360 ng PET sample crystallized at 133 °C for 1 h on heating and subsequent cooling. The measurements were performed at the scanning rates: 1–150 K/s (9000 K/min)—solid line, 2–550 K/s (33,000 K/min)—dash line, 3–1100 K/s (66,000 K/min)—short-dash line, and 4–2700 K/s (162,000 K/min)—dash-dot line. The inset shows the curves in the glass transition range. The curves for completely amorphous and crystalline PET according to Ref. [30] are shown by dotted lines.

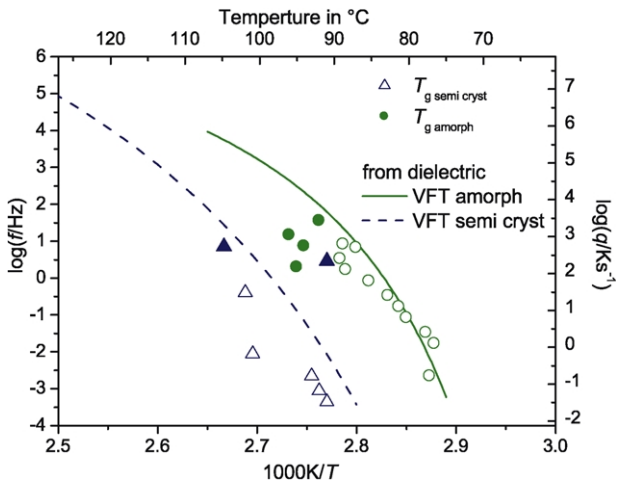

Fig. 5. Activation diagram for amorphous and semicrystalline (crystallized for 1 h at 133 °C) PET. The lines represent VFT fits on the data from dielectric spectroscopy [35]. The points are the glass transition temperatures at different rates from chip calorimetry (solid symbols) and DSC (open symbols). Left axis holds for T_g of the amorphous sample only, see text.

For the thickest sample a well pronounced shoulder appears above 200 °C, while for the thinnest sample basically nothing is seen at such temperatures. Sample thickness of the thinnest sample was about 10 μm. From *trans*-crystallinity studies it is known that layers of such thickness are influenced by *trans*-crystallinity (see e.g. Ref. [37] and references therein). It seems that the morphology in the thinner samples is more stable (does not reorganize as fast) compared to the thicker sample. Because of the different behaviour of the thinner samples we do not discuss the measurements at higher rates here.

In a next step, we measured the melting curves for the three samples after cold crystallization at different temperatures. The curves are shown in Fig. 7.

It seems there is some influence of the sample thickness on the melting behaviour (morphology) as seen in Figs. 6 and 7. The same is true for the heat of fusion. For a 12 mg sample (measured by DSC) heat of fusion equals ca. 45–55 J/g (32–39% crystallinity). The heat of fusion for the 480 ng (24 μm) sample equals ca. 40–50 J/g (29–36% crystallinity, which is similar to the bulk 12 mg sample), for the 360 ng, we measure ca. 35–40 J/g (crystallinity ca. 25–29%) and for the 210 ng sample ca. 30–35 J/g (crystallinity ca. 21–25%) as shown in Fig. 7. This holds except for the samples crystallized at 230 °C where heat of fusion is only about 20 or 10 J/g for the 18 and 10 μm thick samples, respectively.

For the two lowest crystallization temperatures a significant broadening of the high temperature flank for the thick sample is observed. For all other temperatures one single melting peak is seen only. At 230 °C, the crystallization time of 10 h was not long enough to crystallize the samples totally. Actually, the effect is more pronounced for the thinner sample. The presence of a larger amorphous fraction is also seen at the glass transition as a significant higher step in the specific heat capacity, see inset in Fig. 7. Nevertheless, also for these samples a single melting peak is observed only. For the thin sample generally the same behaviour is observed as for the thick sample. As already shown in Fig. 6, the shoulder at the high temperature flank for the melting peaks of the samples crystallized at high super cooling disappears for the thin sample. The other melting peaks become smaller with decreasing sample thickness indicating some influence of the surface on the crystallization process.

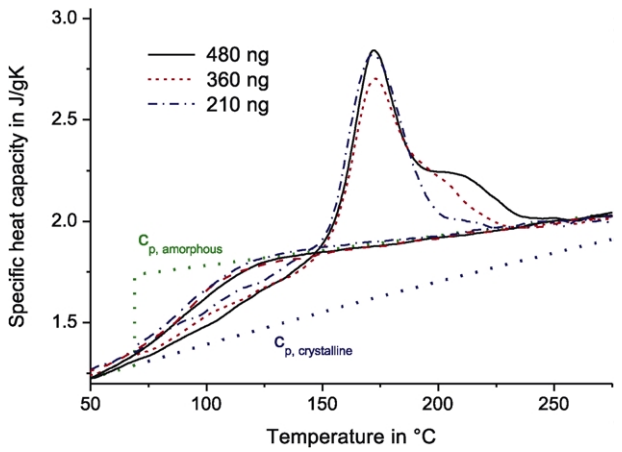

Fig. 6. Temperature dependences of the specific heat capacity on heating and subsequent cooling of the following three samples: 480 ng (ca. 24 μm thick)—solid line, 360 ng (18 μm)—dashed line, and 210 ng (10 μm)—dot-dashed line at the scanning rate 2700 K/s for heating and cooling. The samples were crystallized at $T_C = 114$ °C and $t_C = 10$ h. The curves for completely amorphous and crystalline PET according to Ref. [30] are shown by dotted lines.

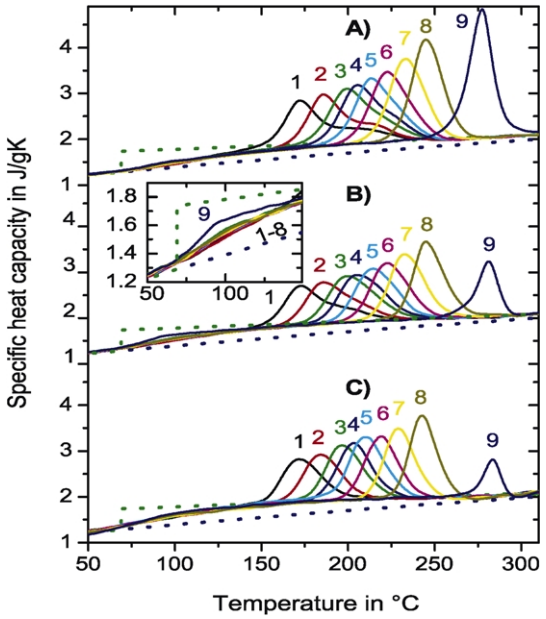

Fig. 7. Temperature dependences of the specific heat capacity of (A) 480 ng (ca. 24 μm), (B) 360 ng (ca. 18 μm) and (C) 210 ng (ca. 10 μm) sample measured at 2700 K/s. The samples were crystallized at $1 - T_C = 114$ °C, $t_C = 10$ h; 2–133 °C, 1 h; 3–153 °C, 15 min; 4–163 °C, 5 min; 5–174 °C, 5 min; 6–185 °C, 5 min; 7–196 °C, 20 min; 8–207 °C, 1 h; 9–230 °C for 10 h. The heat of fusion, ΔH_f, calculated from the area under the melting peak of the curves equals ca. 40–50 J/g for the 480 ng sample, ca. 35–40 J/g for 360 ng sample (except 20 J/g for the highest T_C) and ca. 30–35 J/g for 210 ng sample (except 10 J/g for the highest T_C).

4. Discussion

From DSC and a chip calorimeter we obtained melting curves for isothermally crystallized PET for heating rates ranging from 2 to 162,000 K/min (0.03–2700 K/s). For PET crystallized at 210 °C a heating rate of 200 K/min (3.3 K/s) is high enough to prevent recrystallization during the scan totally, see Fig. 8(A). With increasing super cooling (lower T_c) higher and higher rates are needed to prevent recrystallization during the scan. To illustrate the behaviour, we combine DSC and chip calorimeter results for the samples crystallized at 210 and 130 °C in Fig. 8.

At increasing heating rate for both crystallization

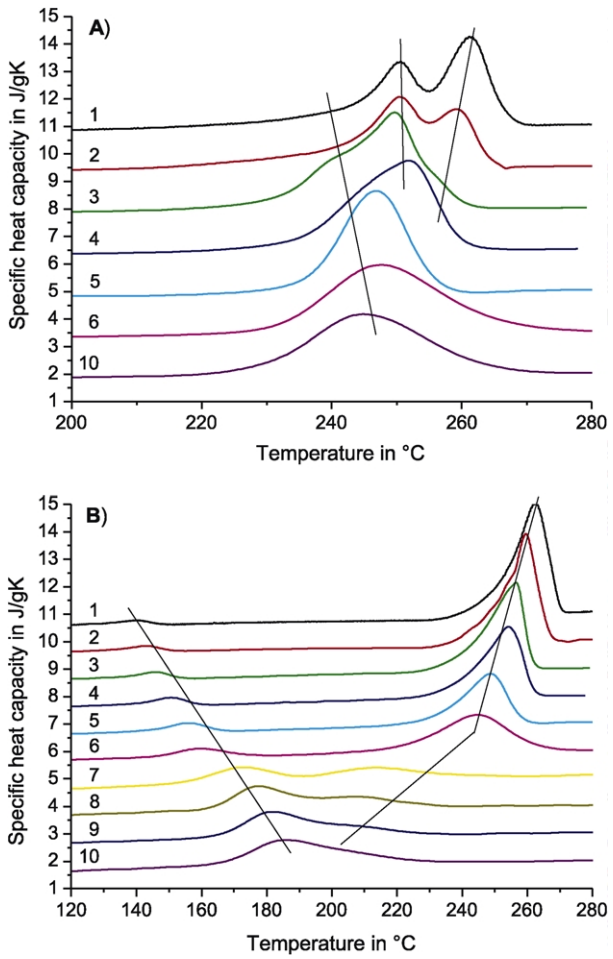

Fig. 8. Temperature dependences of the specific heat capacity of 0.0005–16 mg PET samples at the following heating rates: 1–2 K/min (0.033 K/s) 16 mg, 2–5 K/min (0.083 K/s) 16 mg, 3–20 K/min (0.33 K/s) 6 mg, 4–50 K/min (0.83 K/s) 6 mg, 5–200 K/min (3.3 K/s) 0.5 mg, 6–500 K/min (8.3 K/s) 0.5 mg, 7–9000 K/min (150 K/s), 480 ng, 8–33,000 K/min (550 K/s) 480 ng, 9–66,000 K/min (1100 K/s) 480 ng, 10–162,000 K/min (2700 K/s) 480 ng. The samples were crystallized at 210 °C (A) and 130 °C (B) for 1 h. The curves are vertically shifted and the straight lines are guides to the eyes only.

temperatures the second peak is reduced and shifted to lower temperatures, while the low temperature peak increases in area and finally takes over the whole melting enthalpy. This observation is just as expected from a melting–recrystallization–remelting model. The situation is schematically shown in Fig. 9

Let us assume the melting curve at 162,000 K/min represents the 'true' melting of the crystals formed at isothermal crystallization. This endothermic contribution is then present in the DSC curve too. In the slow DSC curve, we see the beginning of the melting, similar to the curve at fast scanning. But as soon as the first crystals are molten they recrystallize and contribute with an exothermic effect to the heat flow rate measured by DSC. In Fig. 9 it is assumed that the molten crystals recrystallize only once. In reality, the recrystallized fraction will melt and recrystallize at slightly higher temperature again. This way a continuous

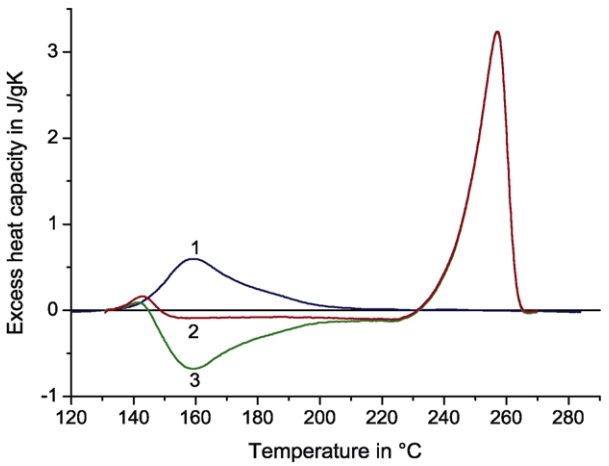

Fig. 9. Excess heat capacity for a PET sample isothermally crystallized at 133 °C for 1 h. 1—Fast scan at 162,000 K/min (2700 K/s), 2—DSC curve at 10 K/min (0.17 K/s), 3—The difference between both measurements showing the exothermic recrystallization. The curve at 162,000 K/min is roughly corrected for super heating.

melting–recrystallization–remelting process occurs yielding a small exothermic net heat flow rate as seen in the flat portion of the DSC curve. Although this model was proposed long time ago [38,39] our fast heating experiments allow us, for the first time, to prove it directly. For PET isothermally crystallized between 114 and 230 °C the model describes the observed behaviour correctly.

The peak temperature of the low melting peak depends strongly on heating rate. This is because the peak temperature equals the temperature where the difference between melting and recrystallization rate is maximal. At slightly higher temperatures—when the heat flow is close to zero—a steady-state regarding melting and recrystallization is established. At low rates, as long as a second melting peak is observed, the maximum is not at all related to some maximum in the lamella thickness distribution as considered for the construction of a Hoffman–Weeks plot [40]. See also a detailed discussion by Yamada et al. [41,42]. Very high heating rates are needed to prevent recrystallization during the melting of PET and to obtain a meaningful melting temperature for the lamellae formed at isothermal crystallization. Under conditions of fast heating superheating has to be considered too. It is, therefore, from a technical point of view alone very questionable if a Hoffman–Weeks extrapolation can give correct values for the equilibrium melting temperature of PET.

In the literature, one can find a large number of papers dealing with the interpretation of temperature modulated DSC measurements in the melting region of polymers [13,43]. Generally a large exothermic contribution is found in the so called non-reversing heat flow close to the beginning of the high temperature melting peak, which is interpreted as a consequence of a large amount of reorganizing material. From our measurements, it follows that reorganization starts already just after the beginning of the melting at low temperature. From Fig. 9, we see that all crystals

undergo recrystallization at least once below 210 °C. This is not at all seen in the TMDSC curves. What is seen in TMDSC is that close to the final melting peak recrystallization becomes slower and comparable with the modulation frequency. If the time scale defined by the modulation coincides with the process under investigation it contributes to the TMDSC signals. This shows again that frequency is the most important factor in TMDSC, which is, unfortunately, very often neglected. The influence of crystallization temperature on the rate of recrystallization is directly seen in Fig. 8. For the sample crystallized at 210 °C the recrystallization rate is so slow that 200 K/min (3.3 K/s) is fast enough to prevent recrystallization. On the other hand the sample crystallized at 130 °C is recrystallizing so fast that even 162,000 K/min (2700 K/s) is not fast enough to prevent recrystallization totally.

Having a tool in hand to study the melting of isothermal crystallized PET without interference of recrystallization allows us to address some more detailed questions. These are (i) what time is needed for reorganization and (ii) can we directly measure the superheating of the polymer crystals?

Analyzing the curve of the thickest sample in Fig. 6 yields some fraction of reorganized material also at a heating rate of 2700 K/s. Let us assume the material recrystallizing is that melting first around 150 °C. The first melting of recrystallized material is observed at about 190 °C. The time needed for the temperature increase of 40 K is about 15 ms at heating rate 2700 K/s. This way, we estimate the time the sample stays between first melting of the original structure and the beginning of the melting of the reorganized crystals. The latter one is not well defined and the estimate can be considered as the maximum time needed for recrystallization. Most probably the process is even faster for the sample crystallized at large super cooling. From our experiment, we have direct evidence that reorganization occurs at a time scale of the order of 10 ms even though crystallization needs much longer time. This result supports the model that there is some remaining order in the melt just after melting a polymer crystal. This ordered melt allows a rapid formation of more stable structures (higher melting temperature) as the original ones. The kinetics of these processes are now available with the fast scanning and isothermal chip calorimeter too because well defined temperature time profiles including cooling steps can be realized with millisecond time resolution [26]. The kinetics of the reorganization will be discussed in more detail elsewhere [44].

The second question, if super heating can be observed directly, is not as easy to answer. This is mainly due to the fact that the hot junctions of the thermopile are about 50 μm apart from the heated area of the sensor. To obtain sample temperature needs, therefore, extensive modeling of the heat flow through the sensor membrane, the gas and the sample. All together an uncertainty of about ±10 K has to be taken into account, as estimated from the measured glass transitions for the amorphous sample. In Fig. 8 the rising flanks of the first melting peak at 2 and 162,000 K/min are shifted for about 30 K. This is significantly larger than the uncertainty of the temperature measurement. The observed shift of 30 K corresponds to a delay of melting of the order of 10 ms.

Schawe [45] proposes 0.45 as the slope for the superheating versus square root of heating rate in K/min for syndiotactic polypropylene. We get 0.05 as the slope, significantly different form Schawe's result. Toda [46] got from DSC measurements for PET $\Delta T_{\text{superheating}} \sim (4\text{K})q^{0.15}$ where q is heating rate divided by K/s. This yields $\Delta T_{\text{superheating}} \approx 13$ K at 2700 K/s in good agreement with our data. Thus, it was possible to observe super heating directly, although the accuracy for the absolute temperature measurement was not very good.

5. Conclusion

Fast scanning calorimetry utilizing a thin film vacuum gauge as calorimeter in combination with conventional DSC covers a scanning rate range between 10^{-4} and 10^{4} K/s. These 8 orders of magnitude allow studying the kinetics of different processes. Our results on melting at rates as high as 2700 K/s give clear evidence for the validity of a melting–recrystallization–remelting process for PET at low scanning rates (DSC). At isothermal melt crystallization PET forms crystals, which all melt within a few dozens of K slightly above the isothermal crystallization temperature. There is no evidence for the formation of multimodal distributions of crystals with different stability (melting temperatures) at isothermal crystallization of PET. The single broad melting peaks at high heating rates show that broad monomodal distributions of lamellae thickness exist. This is in agreement with microscopic and scattering results by Haubruge et al. [47]. Superheating of the crystals is of the order of 10 K at 2700 K/s. Next, we will investigate the melting of polymers for which populations of lamellae with different stability are assumed as the reason for the multiple melting peaks, like isotactic polystyrene (iPS) [15].

Acknowledgements

This work was financially supported by the German Science Foundation (DFG) Grants Schi 331/7, 436 RUS 17/49/03 and PerkinElmer Inc. We acknowledge valuable discussions with M. Merzliakov, Lubbock, TX, USA, L. Allen, Urbana, IL, USA and V. Mathot, Geleen, Nl.

References

[1] Storks KH. J Am Chem Soc 1938;60:1753.
[2] Strobl G. Eur Phys J E 2000;3:165–83.
[3] Lotz B. Eur Phys J E 2000;3:185–94.

[4] Cheng SZD, Li CY, Zhu L. Eur Phys J E 2000;3:195–7.
[5] Muthukumar M. Eur Phys J E 2000;3:199–202.
[6] Sommer JU, Reiter G. Polymer crystallization—obervations, concepts and interpretations. Berlin: Springer; 2002.
[7] Al-Hussein M, Strobl G. Eur Phys J E 2001;6:305–14.
[8] Beekmans LGM, van der Meer DW, Vancso GJ. Polymer 2002;43:1887–95.
[9] Ivanov DA, Amalou Z, Magonov SN. Macromolecules 2001;34:8944–52.
[10] Beekmans LGM, Vancso GJ. Polymer 2000;41:8975–81.
[11] Jiang Y, Yan DD, Gao X, Han CC, Jin XG, Li L, Wang Y, Chan CM. Macromolecules 2003;36:3652–5.
[12] Sohn S, Alizadeh A, Marand H. Polymer 2000;41:8879–86.
[13] Sauer BB, Kampert WG, Blanchard EN, Threefoot SA, Hsiao BS. Polymer 2000;41:1099–108.
[14] Wang ZG, Hsiao BS, Sauer BB, Kampert WG. Polymer 1999;40:4615–27.
[15] Xu H, Ince BS, Cebe P. J Polym Sci, Part B 2003;41:3026–36.
[16] Holdsworth PJ, Turner-Jones A. Polymer 1971;12:195–208.
[17] Kampert WG, Sauer BB. Polymer 2001;42:8703–14.
[18] Kim HG, Robertson RE. J Polym Sci, Part B 1998;36:133–41.
[19] Pijpers MFJ, Mathot VBF, Goderis B, Scherrenberg R, van der Vegte E. Macromolecules 2002;35:3601–13.
[20] Denlinger DW, Abarra EN, Allen K, Rooney PW, Messer MT, Watson SK, Hellman F. Rev Sci Instrum 1994;65:946–58.
[21] Lai SL, Ramanath G, Allen LH, Infante P, Ma Z. Appl Phys Lett 1995;67:1229–31.
[22] Efremov MY, Warren JT, Olson EA, Zhang M, Kwan AT, Allen LH. Macromolecules 2002;35:1481–3.
[23] Efremov MY, Olson EA, Zhang M, Allen LH. Thermochim Acta 2003;403:37–41.
[24] Efremov MY, Olson EA, Zhang M, Zhang Z, Allen LH. Phys Rev Lett 2003;91:85703.1–85703.1–4.
[25] Adamovsky SA, Minakov AA, Schick C. Thermochim Acta 2003;403:55–63.
[26] Adamovsky SA, Schick C. Thermochim Acta 2004; doi:10.1016/j.tca.2003.07.015.
[27] http://www.xensor.nl/.
[28] Hatta I, Minakov AA. Thermochim Acta 1999;330:39–44.
[29] Minakov AA. Thermochim Acta 2000;345:3–12.
[30] Wunderlich B. Pure Appl Chem 1995;67:1019–26. http://web.utk.edu/~athas/.
[31] Olenka L, da Silva EN, dos Santos WLF, Rubira AF, Muniz EC, Medina AN, Cardoso LP, Baesso ML, Miranda LCM, Bento AC. Anal Sci 2001;17:387–9.
[32] Birge NO, Nagel SR. Phys Rev Lett 1985;54:2674–7.
[33] Donth E. Relaxation and thermodynamics in polymers, glass transition. Berlin: Akademie Verlag; 1993.
[34] Hensel A, Schick C. J Non-Cryst Solids 1998;235-237:510–6.
[35] Dobbertin J, Hensel A, Schick C. J Therm Anal 1996;47:1027–40.
[36] Weyer S, Merzlyakov M, Schick C. Thermochim Acta 2001;377:85–96.
[37] Nitta KH, Yamamoto Y. e-Polymers 2003;024:1–11.
[38] Todoki M, Kawaguchi T. J Polym Sci, Part B 1977;15:1067–75.
[39] Qiu G, Tang ZL, Huang NX, Gerking L. J Appl Polym Sci 1998;69:729–42.
[40] Hoffman JD, Weeks JJ. J Res Natl Bur Stand-A Phys Chem 1962;66:13–28.
[41] Yamada K, Hikosaka M, Toda A, Yamazaki S, Tagashira K. Macromolecules 2003;36:4790–801.
[42] Yamada K, Hikosaka M, Toda A, Yamazaki S, Tagashira K. Macromolecules 2003;36:4802–12.
[43] De Clerck K, Rahier H, Van Mele B, Kiekens P. J Appl Polym Sci 2003;89:3840–9.
[44] Minakov AA, Mordvintsev DA, Schick C. Faraday Discussion 128. Submitted for publication.
[45] Schawe JEK, Strobl GR. Polymer 1998;39:3745–51.
[46] Toda A, Hikosaka M, Yamada K. Polymer 2002;43:1667–79.
[47] Haubruge HG, Jonas AM, Legras R. Macromolecules 2004;37:126–34.